3

Synthesis of Carbon Nanostructures by Microwave Irradiation

J. Vivas-Castro[1], G. Rueda-Morales[1], G. Ortega-Cervantez[1], J. Ortiz-López[1], L. Moreno-Ruiz[2] and M. Ortega-Avilés[2]
[1]*Escuela Superior de Física y Matemáticas, Instituto Politécnico Nacional,*
[2]*Centro de Nanociencias y Micro-Nanotecnologías, I.P.N.,*
Mexico

1. Introduction

Carbon nanotubes (CNT) have been synthesized with various techniques of which the most common ones are laser ablation, electric arc discharge, and chemical vapor deposition. These methods produce CNTs with different characteristics, sometimes involving complex experimental setups that add to their cost of production. It is of current general interest the development of new techniques for the efficient and selective synthesis of CNTs and other carbon nanostructures at the cheapest possible cost. One such possibility is the use of microwave radiation, which over the past few years has played an important role as a thermal tool in organic synthesis due to considerable advantages over conventional methods (Lidström, et al., 2001). The use of microwave radiation in the synthesis and functionalization of carbon nanotubes or other nanostructures is advantageous because it provides a fast and uniform heating rate that can be selectively directed towards a targeted area. The first report of the production of carbon nanostructures with microwaves was made by Ikeda et al (Ikeda et al., 1995), who synthesized fullerenes from microwave-induced naphthalene-nitrogen plasma at atmospheric pressure inside a cylindrical coaxial cavity. O. Kharissova has reported the synthesis of vertically aligned carbon nanotubes using a domestic microwave oven (Kharissova, 2004).

Graphite is a good microwave radiation absorber. It has been used in military applications as radar-absorbing material and in anti-electromagnetic interference coatings for civil purposes. Milled flake graphite and carbon nanotubes have microwave absorption maxima in the 10-15 GHz frequency range (Fan et al., 2009). Microwave radiation can heat or cause arcing in many objects and powdered samples can absorb such radiation and be heated efficiently. Short-time direct exposure to microwave irradiation has been used to produce exfoliated graphite as well as to reduce graphite oxide (Zhu et al., 2010).

In graphite powder, absorbed microwave radiation is converted into heat via dielectric loss and conductive loss mechanisms. Graphite powder is oxidized by long exposure to ambient air and may become partly electrically insulating. Microwaves are absorbed with energy dissipation through the coupling of the radiation electric field with local electric dipoles associated with structural defects in graphite powder particles such as particle edges, dangling bonds, C-O bonds, impurities and others. The electric field of microwaves also drives electric currents with efficient generation of heat due to the highly diffusive transport

of π electrons within small defective graphite particles loosely interconnected between each other.

In this work, we present results on the synthesis of various carbon nanostructures under different preparation conditions using a domestic microwave oven as energy source. Starting material is a mixture of graphite powder with iron acetate which is then subjected to microwave irradiation under different conditions. Heating of mixed powders under microwave irradiation decomposes iron acetate leaving small Fe particles that act as catalysts for the synthesis of carbon nanostructures. Various nanostructures are obtained depending on the way the starting material is prepared and exposed to microwaves as well as on the time of exposure. We make a detailed description of the synthesis results in dependence of those parameters. With this technique, we have obtained blocks of dense arrays of aligned multiwall carbon nanotubes, disordered nanotubes intercalated in between graphite planes, long iron-filled multiwall carbon nanotubes, and other peculiar formations. In addition, we propose mechanisms to explain how the synthesis of these nanostructures takes place.

2. Experimental methods and materials

All the material obtained in this work was produced with the aid of a conventional domestic microwave oven operating at 2.45 GHz (12 cm wavelength) with 1000 W power. Starting material was prepared by mixing 30 wt% of iron (II) acetate (ferrous acetate, $Fe(CO_2CH_3)_2$) from Sigma-Aldrich (99.999% purity) with 70 wt% graphite powders (99.99% purity, particle size less than 75 μm). The powders were then mixed and placed inside quartz ampoules (8 mm inner diameter, 10 cm long) which were then sealed under vacuum (10^{-4} torr).

Temperature of microwave-irradiated ampoules rapidly rises and stabilizes within an elapsed time (few seconds) that depends on sample mass. The final temperature correlates linearly with total mass. It has been reported that 0.25 g of graphite powder irradiated inside a 700 W microwave oven reaches about 1000 °C in 12 seconds (Curling et al., 2009). Microwave irradiation decomposes iron acetate into small Fe particles and at the same time produces thermal swelling of graphite particles inside the ampoules. Various molecular species resulting from thermal decomposition of the iron acetate molecule participate in the chemical reduction of the oxide layer that forms on the surface of graphite and metallic particles and make them catalytically active. Once formed, small Fe particles will also absorb microwave radiation (Liu et al., 2006) and participate in further heating the powder mixture. At initial stages of irradiation, metallic particles are small and eventually coalesce into larger ones. At the same time, they will combine with graphite to form iron carbide from which various nanostructures are generated. Evaporation of the catalytic metal will occur in the case of direct exposure to microwaves because inside the ampoules the mixed powders reach high enough temperatures. Evaporated iron will ultimately condense on the ampoule walls and act as catalyst for the growth of dense arrays of aligned nanotubes.

Quite different products may be obtained by variations in the preparation conditions. We have applied the following: (a) quartz ampoules containing the mixed powders may be sealed under ambient air or under vacuum; (b) the ampoules can be partially submerged in water inside the oven to avoid excessive heating and exposure to microwaves, and (c) direct exposure of the ampoules to microwaves during short periods.

The resulting material was analyzed with scanning electron microscopy (SEM) using a FEI-Sirion instrument operated at 5 kV with secondary electrons. Scanning-transmission

electron microscopy (STEM) was performed with a FEI Quanta Dual Beam instrument. Transmission electron microscopy (TEM) was also employed for the analysis using a JEOL 200 C (200 kV) instrument as well as a FEI-Titan 80-300 with spherical aberration correction (Cs TEM). For determination of the crystalline structure of metal particles inside MWNTs, a double-tilt TEM sample holder was used. For examination with Raman scattering spectroscopy we used two instruments: a Perkin-Elmer Raman Station 400F and a Horiba Jobin Yvon LabRam HR800. For SEM and Raman studies, samples were analyzed 'as grown' with no special preparation. For TEM analysis, suspensions were prepared either in dichloroethane or in deionized water with 0.5 wt% SDBS (dodecylbenzenesulfonic acid) surfactant. To optimize dispersion of sample particles, the suspensions were sonicated in an ultrasonic bath or using a 750 watt ultrasonic tip (Sonics) and later were centrifuged at 16,000 rpm. Samples for STEM and TEM analysis were taken from the supernatant material and deposited by dripping in 300 mesh holey carbon TEM copper grids.

3. Description of synthesized material

3.1 Irradiation of quartz ampoules partially submerged in water

To retard sample reactions, we avoided direct microwave irradiation of the mixed powders by partially submerging the prepared ampoules in water. In this way, most of microwave radiation is absorbed by water and only a fraction of the radiation acts on the sample. The consequence of this is that the material temperature rises more slowly and reactions in the synthesis process will take longer to occur. We estimate that in our case, with our 1000 W oven, the material reaches 1000 °C after 30 minutes. We prepared four samples (all of them evacuated ampoules) with 30, 60, 90 and 120 minutes irradiation time at full power with the turning plate of the oven in operation. Material produced under direct irradiation is distinctly different and will be described separately.

Carbon nanotubes (CNT) grow disorderly on the surface of graphite particles after 30 min irradiation, as can be seen in the particle indicated with the lower arrow in Fig. 1(a). Fig. 1(b) is a magnified view of the same particle where CNTs are clearly seen having curled geometry and a wide distribution of diameters. Statistical analysis in the zone of the sample corresponding to Fig 1(b) reveals that 3% of the tubes have diameters in the 4-10 nm range, 40% in the 10-20 nm range, 25% in the 20-30 nm range and the rest are wider than 30 nm. At this stage, some graphite particles have not completely reacted with iron particles and remain with flat surfaces, as shown with the upper arrow in Fig. 1(a).

In samples with 60 min exposure (Fig. 2), CNTs are more abundant and other types of structures appear. This is the case of Fig. 2(a) where a disordered arrangement of 'worm-like' strips about 0.5 μm wide is observed. Fig. 2(b) shows a magnified view of the zone marked with the rectangle in Fig. 2(a). The worm-like features seem to be formed by small-area graphite layers that have slipped and displaced with respect to each other. Analysis of this sample with transmission electron microscopy reveals the presence of graphite nano particles, graphene layers, encapsulated iron particles inside multiwall carbon nanotubes (MWNT) in different stages of growth, iron-filled graphitic onions and peapod-like structures. Two examples of these structures are shown in Fig. 2(c) and (d). In Fig. 2(c) the arrow marks a series of free graphene layers as a result of exfoliated graphite particles, and Fig. 2(d) marks with an arrow a peapod-like structure inside a double-walled nanotube.

For the sample with 90 min exposure in Fig. 3, curled and disordered MWNTs dominate the type of structures observed as seen in Fig. 3(a). TEM image in Fig. 3(b) demonstrates that these nanotubes are indeed (defective) MWNTs, with irregular number of wavy walls separated 0.34 nm.

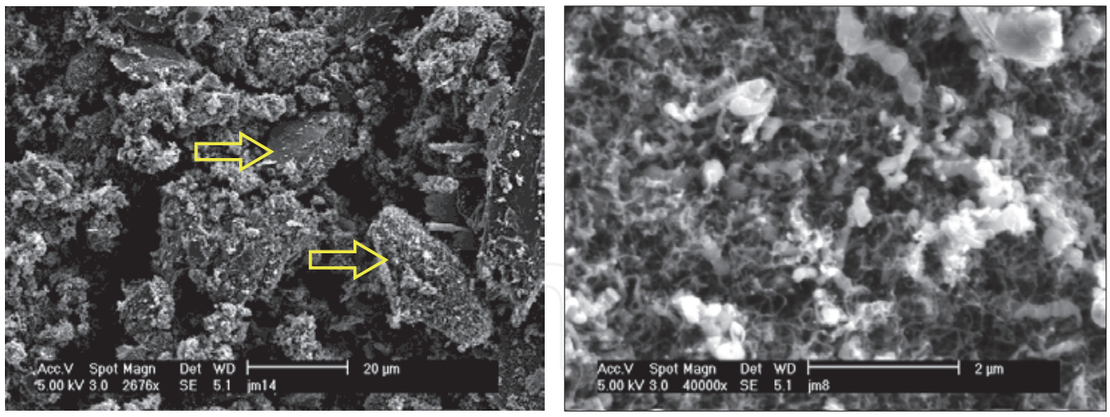

(a) (b)

Fig. 1. SEM images of material obtained in an evacuated ampoule submerged in water after 30 min microwave irradiation: a) view at low magnification; b) view at higher magnification of the surface of particle indicated by lower arrow in (a).

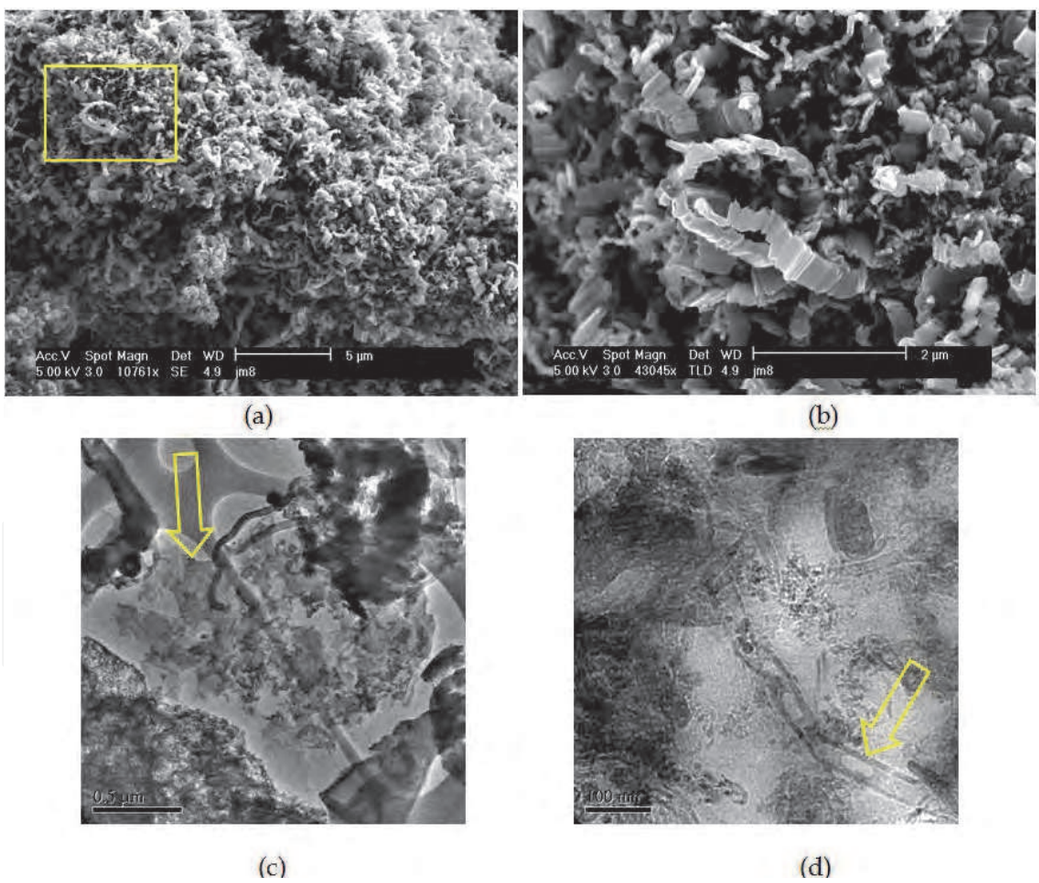

(a) (b)

(c) (d)

Fig. 2. SEM images of material obtained in an evacuated ampoule submerged in water after 60 min microwave irradiation: a) view at low magnification; b) higher magnification of the rectangular zone marked in (a); c) TEM image of graphene layers marked with an arrow; d) TEM image of a peapod-like structure marked with an arrow.

After 120 min irradiation, the majority of the original graphite powder has reacted with iron catalytic particles and has been converted into MWNT. Large (more than 100 μm) and thin (about 2 μm) blocks of disordered MWNTs can be collected on the ampoule walls as seen in Fig. 4(a). The distribution of MWNT diameters falls in the 10-30 nm range. The magnified image of Fig. 4(b) shows a cross sectional view of a fractured block revealing that the blocks are highly porous and have the appearance of metal sponge.

Raman spectroscopy was performed for all samples prepared in evacuated ampoules submerged in water. Their spectra do not display great differences with respect to the irradiation time. Fig. 4(c) shows the Raman response (785 nm excitation, E_{laser}=1.58 eV) of the sample irradiated 120 min which illustrates the typical spectrum observed in other samples. The signal is dominated by a large and wide D-band (1100-1400 cm^{-1}) with a shoulder around 1176 cm^{-1} and a smaller G-band (1500-1700 cm^{-1}). The spectrum has features typical of nano graphite (Pimenta et al., 2007), but in view of our SEM and TEM observations, the signal of a large amount of disordered and defective MWNTs should be also present. A lorentzian line shape analysis reveals some possible component bands as shown in Fig. 4(c). The measured G band has two components, the first one at 1578 cm^{-1}, associated with tangential modes in graphite or MWNT and the second one at 1602 cm^{-1}, to the D´ defect induced band in sp^2 carbons (graphite and MWNTs). The D band can be decomposed in two main components at 1281 and 1310 cm^{-1} as is usual in disordered graphite and MWNTs (Dresselhaus et al., 2005). We identify the shoulder at 1176 cm^{-1} as the manifestation of a weak dispersive mode (sometimes called T-mode) observed in disordered MWNTs, graphite, and other non-planar sp^2 carbons in the 1084-1100 cm^{-1} range (Kawashima, 1995; Li, 1997; Tan, 2004). As seen in our SEM and TEM images, all those types of carbon structures may coexist in our highly inhomogeneous samples.

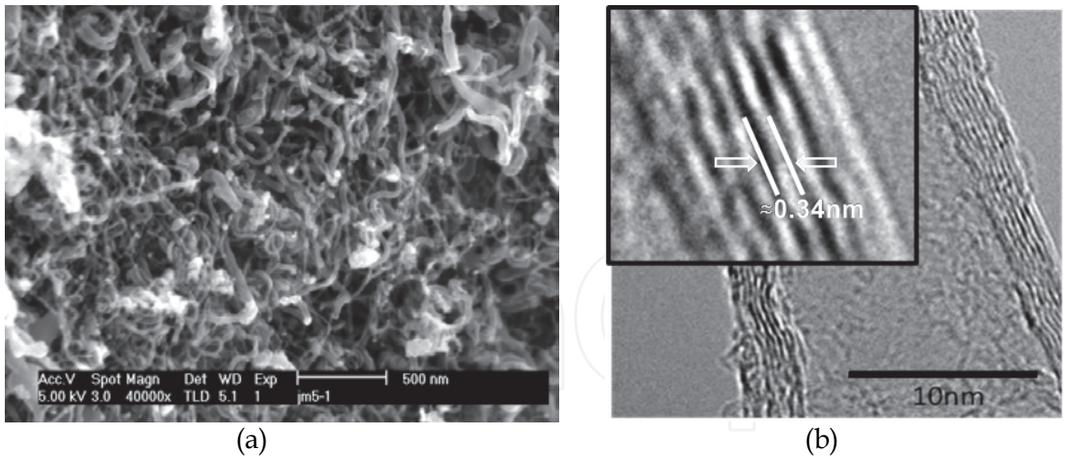

(a) (b)

Fig. 3. Material obtained in an evacuated ampoule submerged in water after 90 min microwave irradiation: a) SEM image of a group of disordered nanotubes; b) TEM image showing that the observed tubes are multiwall; the insert shows a magnified view indicating a 0.34 nm interwall separation.

In samples obtained from ampoules submerged in water, small iron particles are attached to the tips of the observed MWNTs, as shown in the TEM image of Fig. 5. For samples prepared under direct irradiation, higher temperatures and stronger temperature gradients induce complete filling of MWNTs interior with metallic iron as described in next section. In

Fig. 5(a) we observe an elongated iron particle (16 by 28 nm in size) attached to the end of a MWNT and covered by several graphitic layers. Few new layers are seen forming inside the tube as the MWNT grows behind the tip. For the same sample, Fig. 5(b) shows of a group of MWNTs of various diameters, some of them as wide as 50 nm and others as thin as 10 nm, the latter ones with an iron particle at their tip.

3.2 Direct irradiation of quartz ampoules

With direct irradiation, temperature of the mixed powders rises rapidly in few seconds. Reactions are very fast and may become so violent that can cause explosion of the ampoules. Care must be taken to avoid accidents for this reason. To perform these experiments we previously determined the sites inside the microwave oven with maximum radiation intensity. The ampoules (all of them evacuated) were placed horizontally, so that their bottom (filled with the powder mixture) coincided with one of these sites.

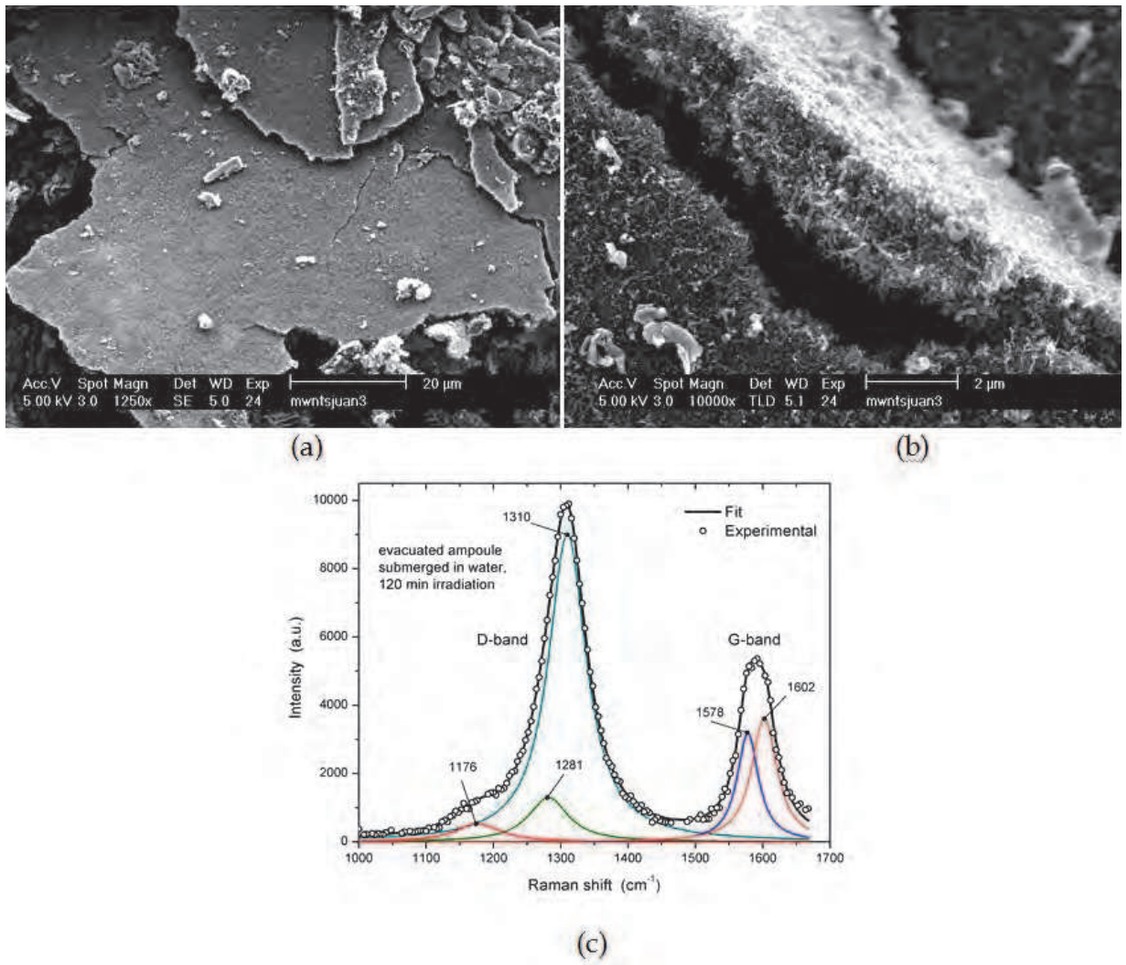

Fig. 4. SEM images of material obtained in an evacuated ampoule submerged in water after 120 min microwave irradiation: a) large blocks of disordered nanotubes collected from the ampoule walls; b) cross sectional view of a fractured block showing that it is entirely composed of disordered MWNTs; (c) Typical Raman spectrum at 785 nm excitation of material obtained after 120 min microwave exposure.

Fig. 6(a) illustrates SEM images of material collected from the ampoule inner walls after 10 min exposure to microwaves. The material is formed by blocks 7 to 10 μm thick of aligned MWNTs also known as CNT 'forests' or 'carpets'. Fig. 6(b), a magnified view of the zone marked with the rectangle in Fig. 6(a), indicates a diameter distribution within the 40-60 nm range. These CNT forests grow from iron particles produced by thermal decomposition of the acetate that accumulate on the inner walls of the ampoules. In Fig. 6(c) we present a Raman spectrum of the same sample. Defect D and tangential G bands are the strongest features of the measured spectrum. The D-band is almost as large as the G-band indicative of a sample with rather defective MWNTs and graphitic particles. At low energy there is a weak feature around 319 cm^{-1} whose nature is unclear but could be attributed either to iron oxide, iron carbide or nano Fe crystals which become Raman active at small size. Another weak and narrow feature can be found at about 1450 cm^{-1}, in between D and G bands, which is identified as an LO or defective mode (Dresselhaus, 2005; Gupta et al., 2006). Other weak features in the Raman spectra of Fig. 6(c) include two small bands, one around 1750 cm^{-1} (M-band) and the other around 1950 cm^{-1} (iTOLA-band). The M-band consists of two components, 1745 and 1788 cm^{-1}, and it has been assigned to an overtone of the infrared-active 'out-of-plane' mode (oTO) at 864 cm^{-1} in sp^2 carbon materials (Brar et al., 2002). The iTOLA-band at 1950 cm^{-1} is identified as a combination of the in-plane transverse optic (iTO) and longitudinal acoustic (LA) modes by the same authors. Other three notorious features are identified as second harmonics and combination modes: (i) at 2427 cm^{-1}, the G*-band which is combination of defective D and T modes; (ii) at 2672 cm^{-1}, the G'-band which is overtone of the D defective mode band, and (iii) at 2927 cm^{-1}, the superposition of the

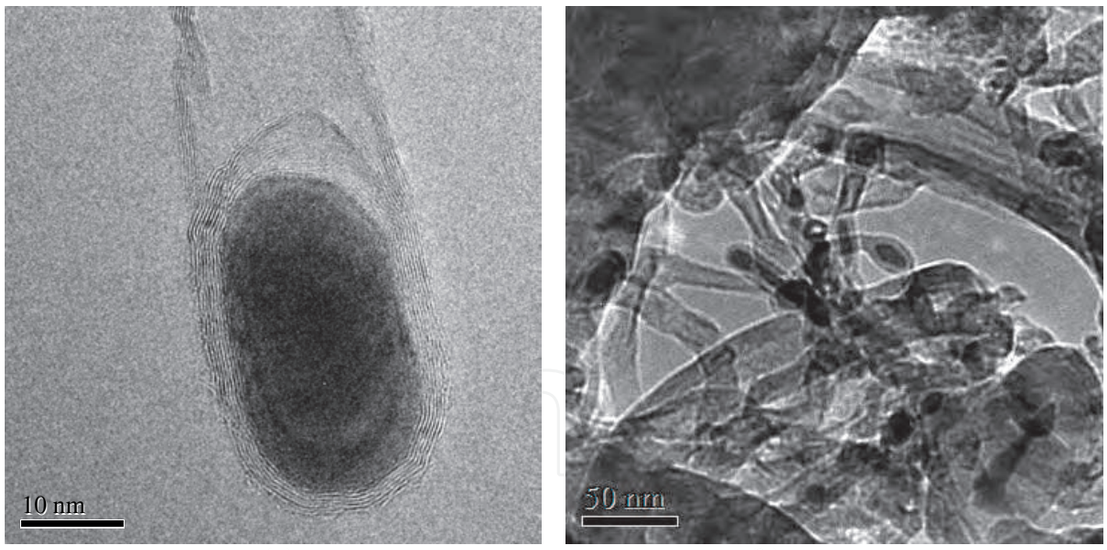

(a) (b)

Fig. 5. TEM images of material obtained in an evacuated ampoule submerged in water after 120 min microwave irradiation a) image of an iron particle at the tip of a MWNT; b) image of a group of MWNTs of various diameters, the narrow ones with an iron particle at their tip.

combined G+D modes and the overtone of the LO mode (Dresselhaus et al., 2005; Kawashima, 1995; Shimada et al., 2005; Sveningsson et al., 2001; Tan, 2004). We note that the 2427 cm^{-1} (G*) band has also been assigned to other combination modes (Maultzsch et al.,

2004) and is usually a weak feature in most sp^2 carbons (Tan, 2004; Yoon, 2009) but in our sample it is rather intense.

Another type of structure that can be obtained is iron-filled MWNTs as shown in the STEM image of Fig. 7(a). The MWNT shown is of about 60 nm external diameter, while the iron filling (in dark trace) is about 2 μm long and 15 nm diameter in its thinnest part. This result was obtained with iron acetate catalyst and direct intermittent exposure to microwaves for an effective time of 15 min. In Fig. 7(b) we present powder X-ray diffraction of the sample corresponding to the image in Fig. 7(a). The identified reflections show the presence of graphite particles (and MWNTs), α-Fe (cubic bcc) and γ-Fe (cubic fcc) crystalline iron as well as iron carbide Fe_3C (cementite), in agreement with nanostructured carbon material synthesized with other techniques (Chen et al., 2004).

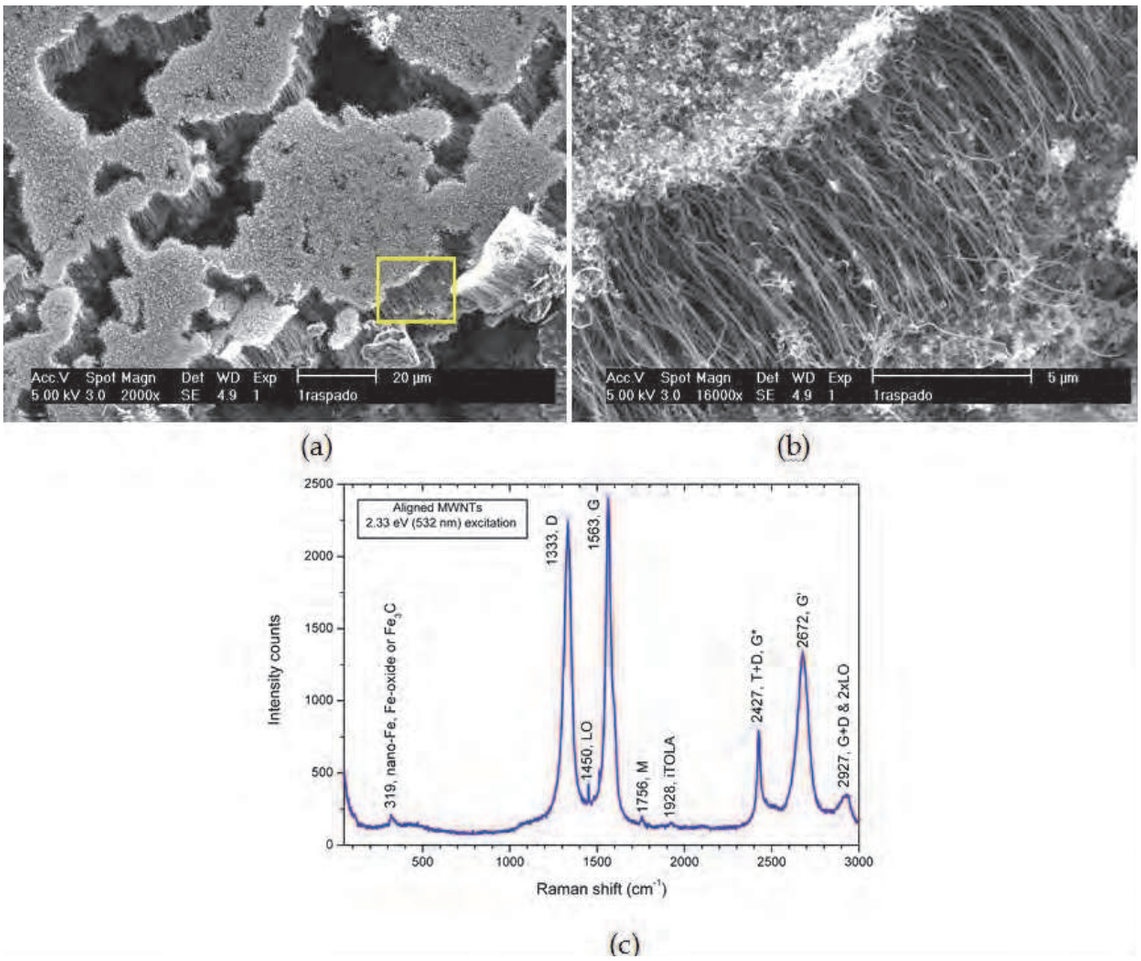

Fig. 6. Material obtained in an evacuated ampoule directly exposed to microwaves for 10 min: a) SEM image at low magnification of parallel arrays of aligned MWNTs; b) higher magnification of the rectangular zone marked in (a); c) Raman spectrum at 532 nm excitation of the same sample.

When the graphite/iron acetate powder mixture is finely ground and thoroughly mixed with mortar and pestle, the time needed of microwave exposure for the synthesis of

nanostructures can be reduced substantially. Seven minutes of irradiation suffice for the appearance of MWNTs and almost complete reaction of the powders. TEM analysis of a sample prepared in this way shows abundant iron filled MWNTs as well as iron particles attached to MWNT tips like the one shown in Fig. 8(a). We chose that particular MWNT for structural identification of the metal particle at the tip using a double-tilt TEM sample holder. The metal particle is relatively large (70 nm wide, 150 nm long) and, as we found from its diffraction pattern, it consisted of several smaller ones of different composition and structure. After few minutes of exposure to the electron beam, the large particle split into smaller ones allowing determination of their individual diffraction patterns from spots close to thin edges. Fig. 8(b) shows the situation after splitting of the original particle and tilting of the sample holder to optimize crystalline orientation respect to the electron beam. Various spots around particle edges were analyzed in detail. The specific spot marked with the square in Fig. 8(b) is shown magnified in Fig. 8(c), in which crystalline planes of the metal particle are clearly resolved. The area marked with the square in this image is further magnified and shown in the inset at the upper left corner in Fig. 8(c). Below this magnified view, its Fourier transform is also shown as inset in Fig. 8(c). The measured interplanar distance is of 2.12 Å in the high resolution image of the inset, and the Fourier transform identifies the crystalline structure as bcc oriented in [110] direction. From this we determine that the particle corresponds to an α-Fe nanoparticle. From analysis of other spots we also find γ-Fe nanoparticles (fcc structure) oriented in [111], as well as Fe_3C nanoparticles (orthorhombic structure). These results are in agreement with chemical analysis by energy

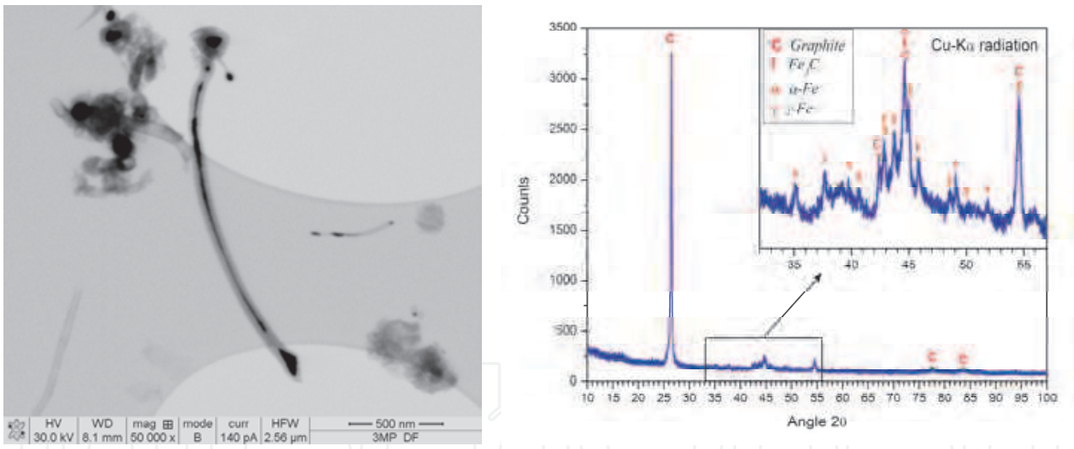

(a) (b)

Fig. 7. a) STEM image of iron-filled MWNTs from samples obtained by direct microwave irradiation; b) X-ray diffraction pattern of sample corresponding to the image in a) in which graphite C, α-Fe, γ-Fe and Fe_3C phases are identified.

dispersive spectroscopy (EDS) which always showed presence of Fe and C and with the X-ray diffraction pattern presented in Fig. 7(b).

4. Mechanisms of nanostructure formation

Both methods of irradiation described in this work result in somewhat different synthesized material. Ampoules submerged in water are dynamically exposed to microwaves with temperature gradients constantly changing because the ampoules themselves are set in

random rocking motion due to the surrounding boiling water. The resulting material in this case are curled MWNTs for long exposure times. In the case of direct irradiation, exposure to microwaves and temperature gradients are static, resulting in the growth of well oriented and aligned MWNTs arrays. In spite of these contrasts, it is possible to elaborate models of the mechanisms involved in the formation of the observed nanostructures.

For initial stages, when temperature is not too high, microwave absorption by graphite particles thermally expands its layers, facilitating the intercalation of foreign species between them (red particles), whilst exfoliation of outermost layers is also taking place. This is described schematically in Fig. 9(a). At the same time, ferrous acetate in our mixed powders is pyrolyzed above 200 °C [1]. Similar as reported for nickel acetate (Afsal et al., 1991), pyrolysis of ferrous acetate proceeds according to the following reactions:

$$Fe(CO_2CH_3)_2 \rightarrow FeO + CH_3COCH_3 + CO_2 \quad (1)$$

$$2\ Fe(CO_2CH_3)_2 \rightarrow 2\ FeO + 2\ CH_3COCH_3 + 2\ CO + O_2 \quad (2)$$

In both reactions, thermal decomposition yields FeO (wustite), and volatile and gaseous components such as acetone CH_3COCH_3, carbon monoxide, carbon dioxide and oxygen. Acetone itself can reduce FeO into metallic Fe which will eventually combine with graphite to form iron carbide Fe_3C (cementite) from which carbon nanotubes and other nanostructures grow. A possible route for this to happen is the following:

$$4\ FeO + CH_3COCH_3 \rightarrow Fe + Fe_3C + 2\ CO + 3\ H_2O \quad (3)$$

Graphite particles in our powder mixture will provide feedstock for the growth of the observed nanostructures either from reaction with metallic Fe or from the carbide Fe_3C obtained from the above reaction. At temperatures above 590 °C, acetone from reactions (1) and (2) may decompose into methane CH_4, ethylene C_2H_2, carbon monoxide and ketene CH_2CO, as reported as early as 1929 (Rice et al., 1929). Methane and ketene may also act as reduction agents of FeO. In relation to pyrolysis of acetone and methane, we should draw attention to the early work of E. L. Evans and collaborators (Evans et al., 1973) who reported the growth of filamentary carbonaceous deposits in the presence of iron, nickel and stainless steel surfaces. In the case of acetone pyrolysis on iron surfaces, these authors found the formation of lamellar γ-Fe_2O_3 at temperatures as low as 400 °C. This last observation indicates that pyrolysis and redox reactions of all chemical species involved may be quite more complex than those implied by the simple reactions (1) - (3).

Metallic particles will interact differently with neighboring graphite grains depending on their relative position respect to the graphite planes (graphene layers). It is expected that catalytic reactivity will be facilitated when the metallic particle sits close to the edges of graphite planes because it will readily interact with carbon end atoms. Evidence of this is seen in the SEM image of Fig. 9(b) where a graphite grain has reacted with iron particles mostly along its flanks (right arrow), while the uppermost layers look unaffected (left arrow). When this occurs, carbon and metallic iron will combine into metallic carbide and a carbon nanostructure will grow from the carbide particle as it becomes saturated with carbon atoms. This growth mechanism for carbon nanotubes is well known in the literature (Saito, 1995). If the metallic particles are small enough (less than 0.7 nm), they will react only

[1]Sigma-Aldrich, material safety data sheet of iron (II) acetate

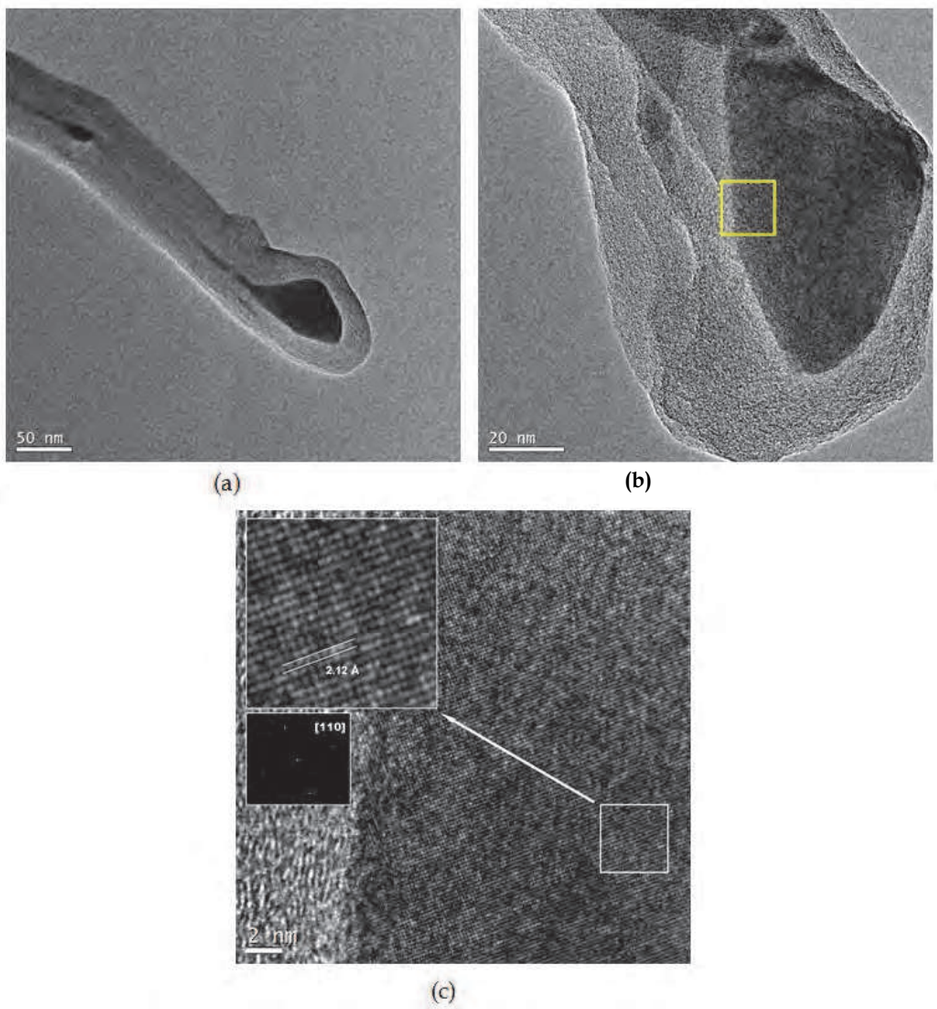

Fig. 8. TEM analysis of metal particle at the tip of a MWNT: a) image of the analyzed particle at low magnification; b) image at higher magnification after splitting of the original particle and tilting of the sample holder; c) higher magnification of the spot marked with the square in (b); inset at the upper left corner is an amplified view of the square marked at the lower right hand side, with its Fourier transform shown underneath.

with a single graphene layer of the graphite particle and may result in an assortment of carbon nanotubes intercalated in between planes of the graphite particle structure. This is schematically illustrated in the drawing of Fig. 9(c) and supported by the SEM image of Fig. 9(d) where a series of disordered nanotubes are seen protruding from amid graphite planes which are normal to the plane of the image and run across the vertically direction. These effects occur at short times of microwave exposure when metallic particles are small. For longer times, metallic particles coalesce into larger ones (red particles in upper drawing of Fig. 9(e), carbon nanostructures emanating from these particles are not drawn) and can interact with more than one graphene layer, leaving unaffected zones of the graphite grains in the form exfoliated graphitic structures, consisting of small-area layers with notorious slippage between each other as indicated in the lower drawing in Fig. 9(e). The SEM image of Fig. 8(f) shows this type of 'worm-like' strips which were already described in Fig. 2(b).

5. Conclusions

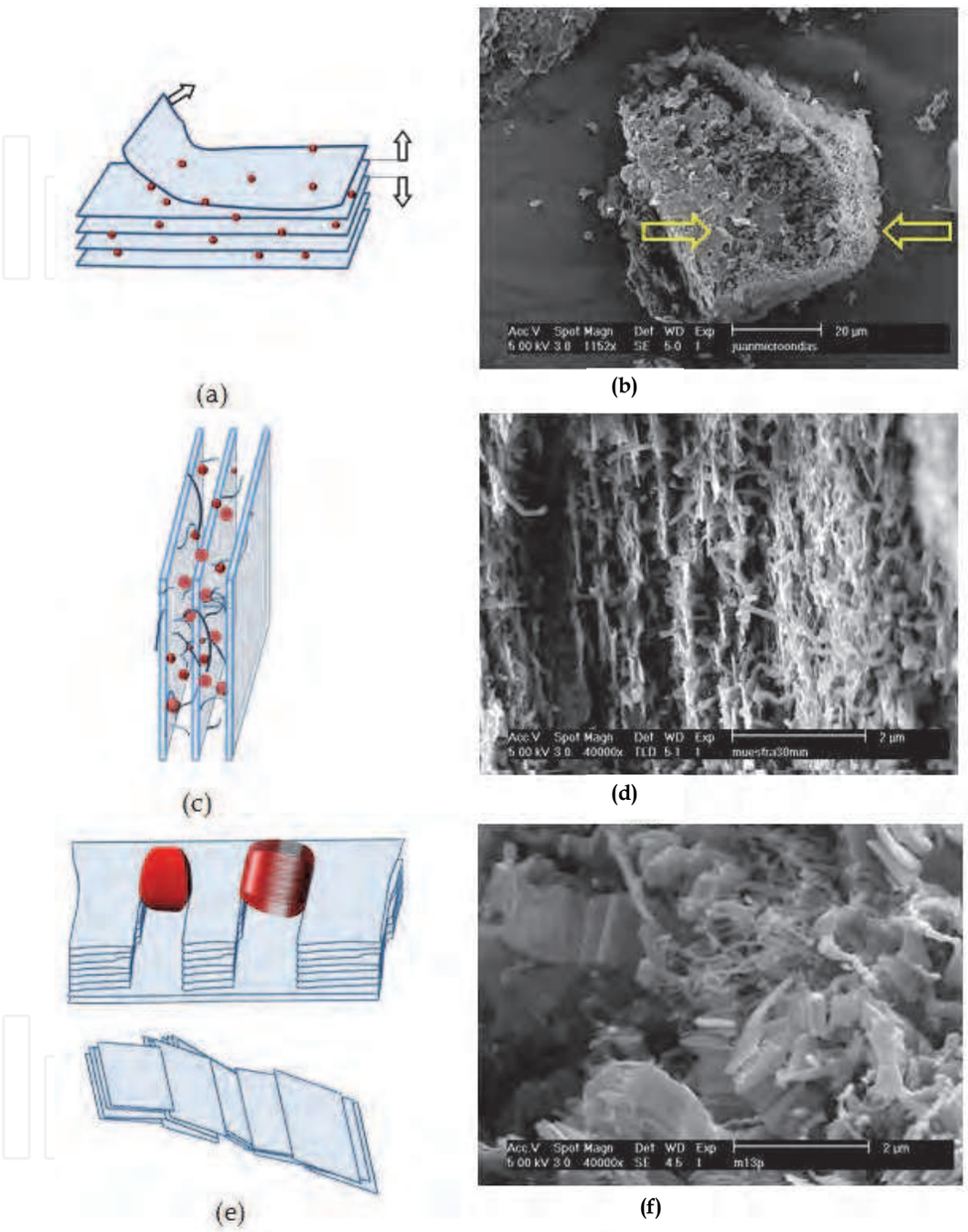

Fig. 9. a) Schematic drawing of expansion, intercalation and exfoliation of graphite particles as consequence of microwave irradiation; b) SEM image showing preferential reaction with iron catalytic particles along the flanks of a graphite particle (right arrow), whilst uppermost layers are almost unaffected (left arrow); c) reaction of small iron particles with individual graphene layers; d) SEM image supporting illustration in (c); e) upper drawing: reaction of large iron particles (red color) with several graphene layers at a time; lower drawing: leftovers of later mechanism leaving 'worm-like' strips of small-area graphene layers with notorious slippage between each other; f) SEM image of 'worm-like' strips illustrated in (e).

The method of synthesis of carbon nanotubes and other carbon nanostructures by microwave irradiation is simple and low-cost. With this technique and under various preparation conditions we obtained nanostructured material from a graphite/iron acetate powder mixture using a commercial microwave oven as energy source. Microwave absorption by the powder mixture results in pyrolysis of iron acetate. Decomposition of the acetate provides metallic iron nanoparticles that act as catalysts in the synthesis of nanotubes and other carbon nanostructures. Different type of nanostructured carbon can be obtained by variation of preparation conditions. Direct irradiation of (vacuum sealed) quartz ampoules, and attenuated irradiation by partial submerging the ampoules in water provide examples of the variety of nanostructures that can be obtained at different stages of microwave exposure. With information collected from these two cases we provide a general explanation of the observed phenomena with a model based on the reaction and exfoliation of graphite powder grains by metallic iron particles. This reaction occurs preferentially on graphene layer edges where carbon end atoms have non saturated dangling bonds. Depending on the size of the iron particle (which depends on effective irradiation time), the interaction will be established with single graphene layers when the particle is small, or with several layers when the particle is large. These conditions will result in the formation of different carbon nanostructures as irradiation time evolves.

6. Acknowledgments

We are thankful to Ing. Daniel Ramirez Gonzalez of IPICYT-Mexico, for TEM analysis of some samples. GRM, GOC and JOL acknowledge support from COFAA-IPN scholarships. GRM, GOC and MOA acknowledge support from EDI-IPN scholarships. JOL acknowledges support from EDD-IPN scholarship. This work was supported by CONACYT-Mexico grant No. 57262 and by SIP-IPN through GRM, GOC and JOL research projects.

7. References

Afzal, M.; Butt, P.K.; Ahrnad, H. (1991). Kinetics of thermal decomposition of metal acetates. *Journal of Thermal Analysis*, Vol. 37, No.5, pp.1015-1023, ISSN 1388-6150.

Brar, V.W.; Samsonidze, Ge.G.; Dresselhaus, M.S.; Dresselhaus, G.; Saito, R.; Swan, A.K.; Ünlü, M.S.; Goldberg, B.B.; Souza Filho, A.G.; Jorio, A. (2002). Second-order harmonic and combination modes in graphite, single-wall carbon nanotube bundles, and isolated single-wall carbon nanotubes. *Physical Review B*, Vol.66, No.15, pp. 155418-155427, ISSN 1098-0121.

Chen, Y.; Conway, M.J.; Fitz Gerald, J.D.; Williamsand, J.M. & Chadderton, L.T. (2004). The nucleation and growth of carbon nanotubes in a mechano-thermal process. *Carbon*, Vol.42, No.8-9, pp.1543-1548, ISSN 0008-6223.

Curling, M.; Collins, A.; Dima, G.; Proud, W. (2009). Progress towards microwave ignition of explosives. *Shock Compression of Condensed Matter-2009*, AIP Conference Proceedings 1195, pp. 486-489, ISBN 978-0-7354-0732-9.

Dresselhaus, M.S.; Dresselhaus, G.; Saito, R. & Jorio, A. (2005). Raman spectroscopy of carbon nanotubes. *Physics Reports*, Vol.409, No. 2, pp. 47-99, ISSN 0370-1573.

Evans, E.L.; Thomas J.L.; Thrower, P.A.; Walker, P.L. (1973). Growth of filamentary carbon on metallic surfaces during the pyrolysis of methane and acetone, *Carbon,* Vol.11, No.5, pp. 441-445, ISSN 0008-6223.

Fan, Y.; Yang, H.; Li, M.; Zou, G. (2009). Evaluation of the microwave absorption property of flake graphite. *Materials Chemistry and Physics,* Vol.115, No.2-3, pp.696-698, ISSN 0254-0584.

Gupta, A.; Chen, G.; Joshi, P.; Tadigadapa, S.; Eklund, P.C. (2006). Raman Scattering from High-Frequency Phonons in Supported n-Graphene Layer Films. A. *Nano Letters*, Vol.6, No.12, pp. 2667-2673, ISSN 1530-6984.

Ikeda, T.; Kamo, T. & Danno, M. (1995). New synthesis method of fullerenes using microwave-induced naphthalene-nitrogen plasma at atmospheric pressure, *Applied Physics Letters*, Vol.67, No.7, pp. 900-902, ISSN 0003-6951.

Kawashima, Y.; Katagiri, G. (1995). Fundamentals, overtones, and combinations in the Raman spectrum of graphite. *Physical Review B*, Vol.52, No.14, pp. 10053-10059, ISSN 1098-0121.

Kharissova, O. (2004). Vertically aligned carbon nanotubes fabricated by microwaves, *Reviews on Advanced Materials Science*, Vol.7, No.1, pp. 50-54, ISSN 1605-8127.

Li, W.; Zhang, H., Wang C.; Zhang, Y.; Xu, L.; Zhu, K.; Xie, S. (1997). Raman characterization of aligned carbon nanotubes produced by thermal decomposition of hydrocarbon vapor. *Applied Physics Letters*, Vol.70, No.20, pp. 2684-2686, ISSN 0003-6951.

Lidström, P.; Tierney, J.; Whatey, B. & Westman J. (2001). Microwave assisted organic synthesis–a review. *Tetrahedron*, Vol.57, pp. 9225-9283, ISSN 0040-4020.

Liu, J.R.; Itoh, M.; Machida, K. (2006) Magnetic and electromagnetic wave absorption properties of α-Fe/*Z*-type Ba-ferrite nanocomposites. *Applied Physics Letters* Vol.88, No.6, pp. 062503-1-3, ISSN 0003-6951.

Maultzsch, J.; Reich, S.; Thomsen, C.; Requardt, H.; Ordejon, P. (2004). Phonon dispersion in graphite. *Physical Review Letters*, Vol. 92, No. 7, pp. 075501-075504 , ISSN 0031-9007.

Pimenta, M.A.; Dresselhaus, G.; Dresselhaus, M.S.; Cançado, L.G.; Jorio, A.; Saito. R. (2007) Studying disorder in graphite-based systems by Raman spectroscopy. *Physical Chemistry Chemical Physics*, Vol.9, No.11, pp. 1276–1291, ISSN 1463-9076.

Rice, F.O.; Vollrath, R. E. (1929). The thermal decomposition of acetone in the gaseous state. *Proceedings of the National Academy of Sciences,* Vol.15, No.9, pp. 702-705, ISSN 0027-8424.

Saito, Y. (1995). Nanoparticles and filled nanocapsules. *Carbon*, Vol.33, No.7, pp. 979-988, ISSN 0008-6223.

Shimada, T.; Sugai, T.; Fantini, C.; Souza, M.; Cançado, L.G.; Jorio, A.; Pimenta, M.A.; Shinohara, R.; Saito, Y.; Grüneis, A.; Dresselhaus, G.; Dresselhaus, M.S.; Ohno, Y.; Mizutani, T. & Shinohara, H. (2005). Origin of the 2450 cm^{-1} Raman bands in HOPG, single-wall and double-wall carbon nanotubes. *Carbon*, Vol.43, No.5, pp. 1049-1054, ISSN 0008-6223.

Sveningsson, M.; Morjan, R.E.; Nerushev, O.A.; Sato Y.; Bäckström, J.; Campbell, E.E.B.; Rohmund, F. (2001). Raman spectroscopy and field-emission properties of CVD-grown carbon-nanotube films. *Applied Physics A*, Vol.73, No.4, pp. 409–418, ISSN 0947-8396.

Tan, P.H.; Dimovski, S.; Gogotsi, Y. Raman scattering of non-planar graphite: arched edges, polyhedral crystals, whiskers and cones (2004). *Philosophical Transactions of the Royal Society A*, Vol.362, No. 1824, pp. 2289–2310, ISSN 1471-2962.

Yoon, D.; Moon, H.; Cheong, H.; Sik Choi, J.; Ae Choi, J.; Ho Park, B. (2009). Variations in the Raman Spectrum as a Function of the Number of Graphene Layers, *Journal of the Korean Physical Society*, Vol.55, No.3, pp. 1299-1303, ISSN 0374-4884.

Zhu, Y.; Murali, S.; Stoller, M.D.; Velamakanni, A.; Piner, R.D.; Ruoff, R.S. (2010). Microwave assisted exfoliation and reduction of graphite oxide for ultracapacitors, *Carbon,* Vol.48, No.7, pp. 2118-2122, ISSN 0008-6223

Carbon Nanotubes - Synthesis, Characterization, Applications
Edited by Dr. Siva Yellampalli

ISBN 978-953-307-497-9
Hard cover, 514 pages
Publisher InTech
Published online 20, July, 2011
Published in print edition July, 2011

Carbon nanotubes are one of the most intriguing new materials with extraordinary properties being discovered in the last decade. The unique structure of carbon nanotubes provides nanotubes with extraordinary mechanical and electrical properties. The outstanding properties that these materials possess have opened new interesting researches areas in nanoscience and nanotechnology. Although nanotubes are very promising in a wide variety of fields, application of individual nanotubes for large scale production has been limited. The main roadblocks, which hinder its use, are limited understanding of its synthesis and electrical properties which lead to difficulty in structure control, existence of impurities, and poor processability. This book makes an attempt to provide indepth study and analysis of various synthesis methods, processing techniques and characterization of carbon nanotubes that will lead to the increased applications of carbon nanotubes.

INTECH
open science | open minds

InTech Europe
University Campus STeP Ri
Slavka Krautzeka 83/A
51000 Rijeka, Croatia
Phone: +385 (51) 770 447
Fax: +385 (51) 686 166
www.intechopen.com

InTech China
Unit 405, Office Block, Hotel Equatorial Shanghai
No.65, Yan An Road (West), Shanghai, 200040, China
中国上海市延安西路65号上海国际贵都大饭店办公楼405单元
Phone: +86-21-62489820
Fax: +86-21-62489821

IntechOpen